Journal of Applied Polymer Science

Impact of organoclays on the phase morphology and the compatibilization efficiency of immiscible poly(ethylene terephthalate)/poly(ε-caprolactone) blends

Dalila Saaoui,[1,2] Samira Benali,[2] Rosica Mincheva,[2] Abderrahmane Habi,[1] Philippe Dubois,[2] Jean-Marie Raquez[2]

[1]Laboratoire des Matériaux Organiques, Faculté de Technologie, Université Abderrahmane Mira, Route de Targa Ouzemour, 06000, Bejaia, Algeria

[2]Center of Innovation and Research in Materials and Polymers (CIRMAP), Research Institute for Materials Science and Engineering, University of Mons- UMONS, Place du Parc 20, B-7000, Mons, Belgium

Correspondence to: S. Benali (E-mail: samira.benali@umons.ac.be)

ABSTRACT: Adding nanofillers Cloisite 30B (C30B) and Cloisite 15A (C15A) to poly(ethylene terephthalate) (PET)/poly(ε-caprolactone) (PCL) (70/30, wt/wt) blends via melt blending can improve their phase morphology and change their interface properties. The effects of the different selective localization of clay on the structure and the morphologies are studied and evaluated by theoretical and experimental methods. It is found that C30B is selectively localized in PET and at the PET-PCL interface, whereas C15A is mainly localized at the interface. Moreover, the changes in the rheological behavior of the blends are attributed to the formation of clay network-like structures. X-ray diffraction, scanning electron microscope, and transmission electron micrograph observations also evidenced an exfoliated and/or intercalated structure of C30B, and intercalated structure of C15A in the blend, together with significant morphology changes of the initially immiscible blend. The relative permeability to PET/PCL of the nanocomposites decreased with the increasing of nanoclays content.
 J. Appl. Polym. Sci. **2020**, *137*, 48812.

KEYWORDS: blends; clay; compatibilization; rheology; structure—property relationships

Received 18 June 2019; accepted 29 November 2019
DOI: 10.1002/app.48812

INTRODUCTION

Poly(ethylene terephthalate) (PET) is a semicrystalline thermoplastic with a high melting point (250 °C) and is widely used in the packaging, biomedical,[1] and textile industries.[2] However, brittleness and poor elongation at break represent important limitations for a most wider application of PET. To overcome these drawbacks, additions of reinforcing fillers and toughening modifiers were already investigated. For example, PET has been blended or compounded with several polymers, fillers, and nanoparticles to modify its physical properties. The addition of a second component to improve the mechanical performance has been reported[2–5] including ductile polymers such as poly(ε-caprolactone)[6] or PBAT poly(butylene adipate-*co*-terephthalate).[2]

Indeed, PCL is a semicrystalline polyester, in which (1) its thermal properties—that is, glass transition and melting temperature—are significantly lower than those of PET, but with comparable thermal resistance and (2) mechanical properties—that is, storage modulus and elongation at break (1906%[7] and 2.2%[8] for PCL and PET, respectively) are completely different and makes it suitable for manufacturing flexible devices. However, the insufficient number of favorable PCL–PET interactions (hydrogen bonds between PCL OH end groups and PET—C(O)O— groups) in the case of blends containing high molar mass PCL, result into only partially miscible blends[9] where the resulting mechanical properties might not be optimal in terms of applications.

Improving the miscibility between polymer pairs can be achieved using different approaches as copolymer formation for example. The process is based on transesterification reactions as catalyzed by the presence of residual polymerization catalysts and to extent after adding an extra amount of transesterification catalysts. This was successfully validated by Jun *et al.*,[10] followed by Lim *et al.*[11] for a blend of PET and PCL homopolymers. Indeed, at the early stage, both homopolymers progressively turned into a random copolymer passing through a block-like structure. However, depending on the extent of transfer reactions, different conclusions on miscibility of the components can be drawn.[9,10] Besides, despite all benefits, the process then brings to worsening the

Additional Supporting Information may be found in the online version of this article.

material performance (mechanical strength, chemical, and thermal resistance)[12] and its applications remain restrained. An alternative is proposed by Hirotsu *et al.*[13] who restricted the melt blending to "intimate" mixing of PET and PCL and then exposed the final blend to plasma treatment. While preserving the properties of the individual polyesters, this method generated microstructures on the surface but could not affect the bulk of the sheets.

As another alternative, Avery largely studied approach relies on the use of inorganic fillers as montmorillonites (nanoclays)[14–19] for modifying the morphology and interfacial properties of blends. The interest on nanoclays comes from their versatility in terms of type, interlayer distance, and hydrophilicity/hydrophobicity that can influence their compatibilization role in most blends.[17] For example, Fang *et al.*,[17] prepared poly(ε-caprolactone)/poly(ethylene oxide) (PCL/PEO) blends containing Cloisite30B (C30B) or CloisiteNa$^+$ as nanofillers and observed that the C30B nanoplatelets were preferentially located at the interface between the PCL and PEO phases with the formation of a network structure. Similar results were obtained by As'habi *et al.*[18] who studied the effect of mixing conditions and the clay type (C30B and C15A) on the morphological, rheological, and degradation behavior of PLA/LLDPE nanocomposites. The results showed that, in comparison with nonpolar C15A, medium-hydrophobic C30B had a strong influence on the size reduction of dispersed LLDPE phase and C30B layers were highly delaminated in the PLA phase. However, and up to our knowledge, studies on the compatibilization of PET/PCL blends using montmorilonites are not yet available in the literature.

After a preliminary study of the best formulation blends (PET/PCL) and the best filler range, not showed here for sake of clarity, we chose to present the investigation results about the role of C30B and C15A (at content of 1, 2, and 3 wt %) on the compatibilization of blends with weight ratio PET/PCL of 70/30.

The C30B was chosen for its affinity to PET[19] and the nonpolar C15A for its long alkyl chain surfactant and high initial gallery spacing. The nanocomposites were prepared using a direct melt blending and their rheological properties and morphology were studied. In parallel, mechanical and CO_2 barrier properties were also measured from packaging prospectives.

MATERIALS AND METHODS

Materials

Commercial-grade PCL (CAPA 6800; number-average molecular weight of 80 000 g mol^{-1} and melting temperature of 58–60 °C) was supplied by Perstorp Chemicals (Belgium). Commercial-grade PET (TexPET Grade-IV 0.62; intrinsic viscosity of 0.8 ± 0.02 dL g^{-1} and melting temperature of 247 °C) was supplied by Kenplast Industry (Nairobi, Kenya). Two types of organoclays were purchased from Southern Clay Products, Inc., under the commercial names of Cloisite30B and Cloisite15A (here after denoted C30B and C15A, respectively). According to the supplier, natural montmorillonite was modified with methyl tallow bis-2-hydroxyethylammonium or with dimethylhydrogenated tallow ammonium to give C30B or C15A, respectively.

Material processing

Prior processing, PET and PCL granules and nanoclays (C30B or C15A) were dried overnight at 80, 60, 40 °C, respectively, under reduced pressure. The neat PET/PCL binary blend with a composition 70 wt %/30 wt % and its nanocomposites containing C30B or C15A at 1, 2, and 3 wt % of inorganic content were prepared in a co-rotating twin-screw extruder (Micro Compounder Xplore Model 15cc 2005) under nitrogen at 260 °C. Screws rotation speed for introducing was fixed to 30 rpm for 2 min and then increased to 100 rpm for 3 min for processing. The extrudates were recovered, cut and dried under vacuum at 60 °C for 12 h, and all specimens were injected at 260 °C and 10 MPa of pressure with a mold at 40 °C for 6 s of cooling time.

Characterization

Rheology was performed on PET/PCL and PET/PCL/organoclay samples. The storage modulus (G'), loss modulus (G''), and the complex viscosity (η^*) were measured as a function of the angular frequency (ω), using an TA instrument ARES rheometer under air after checking that no degradation is occurred (TGA showed in the Supporting Information Figure S4 for sake of the clarity). The limit of the linear viscoelastic regime was determined by performing a strain sweep at 1 Hz. The rheometer was operating in dynamic oscillatory mode with parallel plate geometry of 25 mm diameter at 260 °C. A strain maximum of 10%, chosen from the linear viscoelastic domain, was used to perform dynamic measurements over a frequency range of 100–0.01 Hz. For each material, the results are the average of three experiments.

The morphology of the blends was observed on cryofractured surfaces using a scanning electron microscope (SEM) Hitachi SU8020, with field emission gun with landing energy at 5 kV and SE(UL) detector. Prior analyses, the PCL phase was extracted by dipping in chloroform for 5 min and drying under air for 3 days according to the literature.[20]

The localization and dispersion of the nanofillers were investigated by transmission electron micrographs (TEMs) using a Philips CM200 apparatus at an acceleration voltage of 100 kV.

Morphological X-ray diffraction (XRD) analysis was performed on a Siemens D5000 diffractometer using Cu Kα radiation (wavelength: 1.5406 Å) at room temperature in the range of 1.5°–50°, by step of 0.048, and a scanning time of 28 min.

Tensile properties were measured with Zwick/Roell machine operating at 20 °C with a constant deformation rate of 2 mm min^{-1} according to the ASTM D638 type V norm for dumbbell-shaped specimens (1.5 × 5 mm^2) prepared by injection molding. Tensile data are the average of five measurements.

Gas-transport properties experiments were performed using a gas permeability tester PERMEAVAC-VBS provided by Labthink (China) on compression-molded circular films (200 μm). Samples were prepared using a CARVER (Wabash, IN) laboratory press (260 °C, 5 min, then quenched at 50 °C). Testing is based on the differential pressure method to determine the gas transmission rate of films according to the GB/T 1038-2000 standards. The temperature was controlled at 23 ± 0.1 °C by a constant temperature control device. Before resuming the gas permeation

experiments, the sample was exposed to controlled room conditions (temperature and moisture) for at least 48 h. The measurements were carried out considering a monolayer membrane of thickness l (cm) and surface A (cm^2), submitted to a permeant of total amount Q (cm^3 m^{-2}.d.Pa) passing through during a time t (days). Considering a steady state, the permeant flux density J (cm m^{-2}.d.Pa.days) is given by eq. (1):

$$J = \frac{Q}{A \times t} \quad (1)$$

The flux can be related to the average concentration, C ($mol.L^{-1}$), on both sides of the membrane with a coefficient k—the total mass transfer coefficient across the membrane according to eq. 2:

$$\frac{Q}{t} = k \times (C_1 - C_2) \quad (2)$$

where $C_1 > C_2$.

The transport properties measurements are based on the integral permeation method, which was performed in a closed chamber. The oxygen transmission rate curve reaches asymptotically a maximum value after a certain time and then the permeance can be determined upon the time-lag method from manometric data. The permeance (in cm^3 m^{-2}.Pa^{-1}) was obtained by instrument software. Data were averaged on three samples. Control measurements were conducted on reference film provided by Labthink and the relative error of permeance was found to be less than 5%.

RESULTS AND DISCUSSION

Rheological behavior

In order to study (1) the role of clays (type and loading) on PET/PCL blends compatibilizaiton state and (2) the dispersion state of the nanofillers in the polymeric matrices, the structural change was evaluated via dynamic rheology measurements. For this purpose, C30B or C15A was dispersed at 1, 2, and 3 wt % in PET/PCL (70/30, wt/wt) blends. The storage modulus (*G*') as a function of frequency of the PET/PCL blend and the PET/PCL-based nanocomposites are shown in Figure 1. The results are the average of three measurements and the average error does not exceed 2%.

As shown in Figure 1, while the *G*' of the PET/PCL blend increases steadily with frequency, the slope of the curves decreases with the introduction of nanoclays. Additionally, *G*' increases significantly and presents a frequency independent solid-like behavior at lower frequencies. These effects are independent on filler type and become more pronounced at higher filler loading, thus indicating increased relaxation times and a transition from liquid to solid-like behavior.[17] Similarly to the literature,[17] strong particle–particle interactions and a formation of a three-dimensional network structure as a result of clay exfoliation might be expected. Particle–polymer interactions and orientation effects might also contribute to the good dispersion of nanoclays in the blend.

The dynamic viscosity as a function of frequency of PET/PCL blend with a 70/30 composition and PET/PCL nanocomposites with 1, 2, and 3 wt % of C30B and C15A is given in [Figure 2(a,b)]. The complex viscosity of PET/PCL presented a Newtonian behavior with the appearance of the plateau at the terminal region, followed by shear-thinning behavior at the highest frequencies, which is a typical behavior of polymer materials. The incorporation of commercial organoclays affects significantly the complex viscosity of immiscible PET/PCL blend over the whole frequency range. The viscosity of the nanocomposites is much higher than that of the blend PET/PCL due to the presence of a strong interaction between blend component such as the filler–polymer and filler–filler interactions. Increasing the inorganic content increases the complex viscosity. This enhancement of viscosity is caused by the deformation of the polymer chains imposed by the interaction of clay layers with the polymer chains. The complex viscosity decreased with increasing frequency for both nanocomposites, indicating a non-Newtonian and pseudo plastic behavior.[21]

The authors noted that a small amount of clay (1 wt %) acts as a plasticizer and therefore decreases the complex viscosity. The nanocomposite with lower filler content possesses weak filler–filler interaction[22] and this may result from a more freely rotation and orientation of filler layers when submitted to shear forces.

To further confirm the reinforcement role of the nanoclays, and because the molecular weight of matrices are similar for both 3 wt % nanocomposites compositions, the *G*'(PET/PCL/clay)/

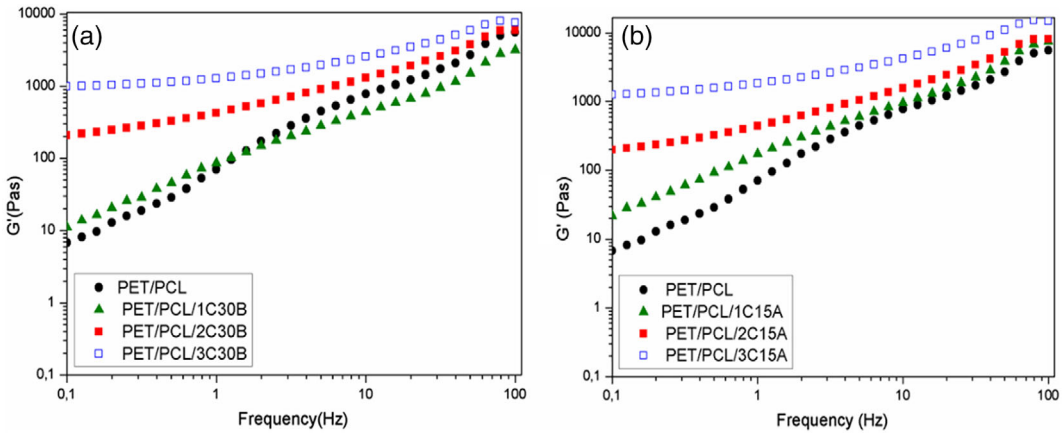

Figure 1. Storage modulus evolution of blends and its nanocomposites prepared with C30 (a) and with C15A (b). [Color figure can be viewed at wileyonlinelibrary.com]

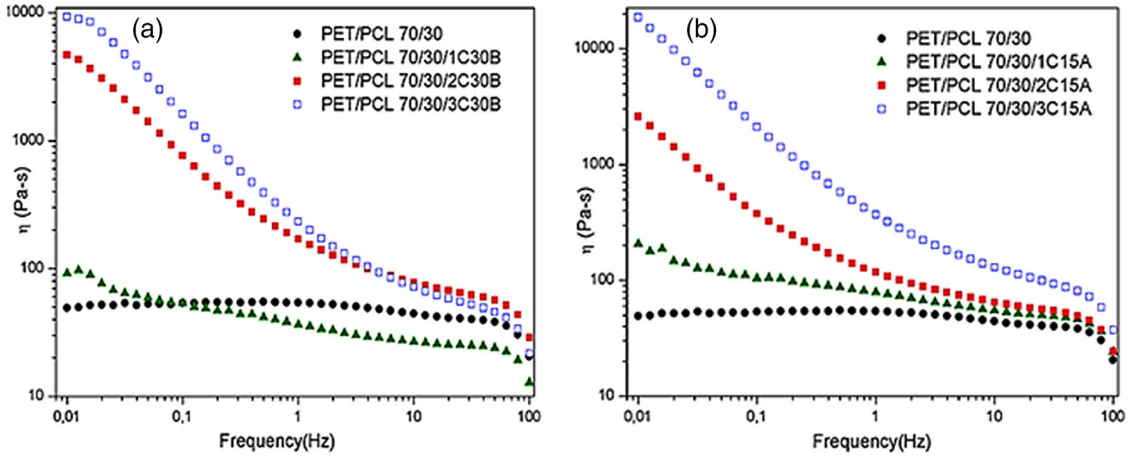

Figure 2. Complex viscosity evolution of blends and its nanocomposites prepared with C30B (a) and with C15A (b). [Color figure can be viewed at wileyonlinelibrary.com]

G'(PET/PCL) as a function of frequency is plotted (Figure 3). In the parallel, a complementary study of the nanoclay reinforcement effect is also reported in the Supporting Information (Figure S1). As might be observed, at a constant filler loading (3 wt %), the curves follow similar behavior independently on filler type. Nevertheless, one can speculate that the reinforcing factor for the nonpolar C15A is higher than for the polar C30B with the effect being more pronounced at higher frequencies. Such results are similar to data obtained for PLA[22,23] and suggest that compatibility mechanism significantly depends on the affinity between the matrix and the nanoclays. However, the initial spacing of the clays must also be taken into consideration.[7]

Additional information about the relaxation behavior and its evolution with filler type and loading was obtained from Cole–Cole plots, in which η" versus η' are shown as a measure of microstructural changes in polymer blends. As known, Cole–Cole plots of miscible blends display a single and smooth semicircular arc-like shape suggested to be a measure of good compatibility between the blended components.[21,24] Deviations from this semicircularity are considered indicative of immiscibility between components of two different relaxation mechanisms or for an "yield behavior"—a change of rheological behavior to solid-like.[21,24] Figure 4 shows the Cole–Cole plot of PET/PCL blend, PET/PCL/C30B (a) and PET/PCL/C15A (b) nanocomposites at different filler content. As it might be seen, the Cole–Cole plot of PET/PCL blend shows two overlapping semicircular arcs, which might be ascribed to a separated relaxation mechanism of one of the two polymer partners, thus confirming the poor compatibility. Similarly, PET/PCL/1 wt % C30B nanocomposite shows two circular arcs accompanied with an upward inflection, suggesting an yield behavior. This inflection is more pronounced for blends containing 2 and 3 wt % of C30B or C15A and suggests a good dispersion state of the clay in PET/PCL matrix accompanied by a better compatibility between the polyesters.[21] Intriguingly, at 3 wt % filler loading and at high frequencies, a trend to forming a semicircular shape in the plot can be observed (Figure 4), suggesting again an improvement of the miscibility of the PET/PCL blend and to the transition from liquid to solid-like viscoelastic behavior. To further confirm the effect of clays loading on the miscibility of the blend components, the morphology of the PET/PCL blends at 3 wt % filler was observed by SEM (Figure 5) and TEM (Figure 6).

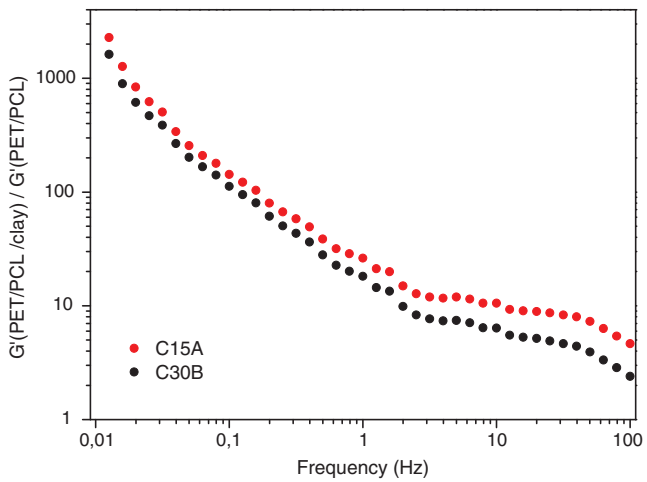

Figure 3. Effect of 3 wt % clay mineral type on the reinforcing factor of PET/PCL/OMMT systems. [Color figure can be viewed at wileyonlinelibrary.com]

Morphology of blends

In order to visualize the rheology-suggested role of clays on the morphology of the blends, cryofractured PET/PCL and PET/PCL/clay (3 wt % of C30B or C15A) surfaces were studied by SEM (Figure 5). In agreement with the literature,[11,20] the SEM images of etched PET/PCL surfaces [Figure 5(a)] showed cavities resulting from PCL extraction, thus confirming the immiscibility of both components in the blend. These cavities became smaller with the addition of C30B and C15A [Figure 5(b,c)], indicating a morphology change into a continuous single phase and improved miscibility of both polymers in the presence of organoclays. We can also observed that the cavities are smallest and fewer with C15A which can be due to a stronger compatibilization. This confirms the rheological data of Figure 3. The observed changes in blends morphology might be explained by (1) an increased

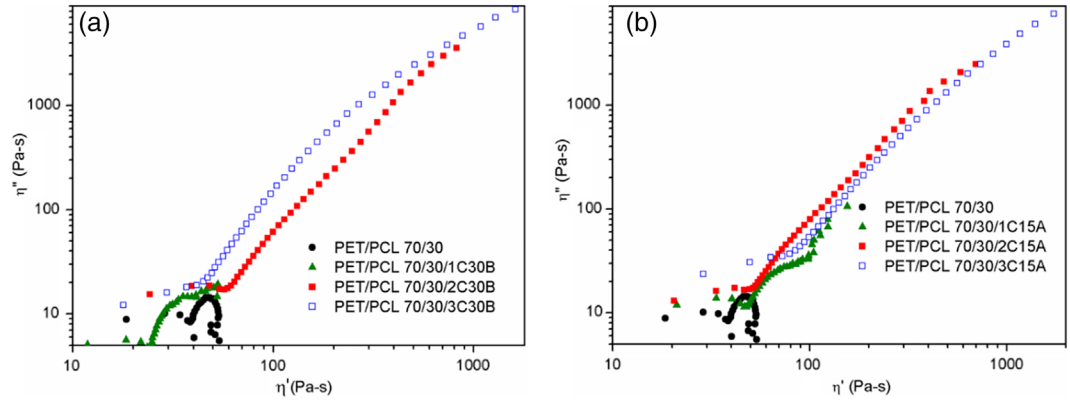

Figure 4. Cole–Cole plot of PET/PCL (a) PET/PCL/C30B and (b) PET/PCL/C15A. [Color figure can be viewed at wileyonlinelibrary.com]

blend viscosity via network formation between the clay sheets (related stress is undergone by the dispersed particles) and/or (2) localization of the filler at the PET/PCL interface (role of "true" compatibilizer).[25] Additionally, according to Figure 5(c), the effect is more pronounced for C15A with comparison to C30B, which might be ascribed to (1) a very high interlayer spacing of the C15A and/or (2) a high concentration of surfactant in C15A.[26] The nonpolar nature of C15A explains the location of organoplatelets at the PET/PCL interface, unlike C30B, which is mainly localized in the PET phase and (to a certain extent) at the PET/PCL interface. This obviously higher affinity of C30B to PET has been studied by Kim *et al.*[27] Hydroxyl groups of C30B could easily interact with polar groups of PET. The observed changes in the PET/PCL blend morphology (Figure 5) upon clay addition might then be explained by the formation of new interface at which interactions between both polymers are ensured by the clay presence. Moreover, the interactions seem modulated by the nature and the amount of clay at the new interface being more pronounced in the presence of C15A (with comparison to C30B).

For clarifying the observed changes in blends morphology, the location of C30B and C15A within PET/PCL blends was studied by TEM (Figure 6). With comparison to the neat PET/PCL blend, where two distinct phases a dark gray and a white are clearly seen in TEM images (Figure 6(a)), the clay-containing nanocomposites show the lateral sections of C30B and C15A [Figure 6(b,c)]. Concerning the phase differentiation in TEM for the neat PET/PCL blend similar effects has already been observed in the literature for PCL/poly(ethylene oxide) blends.[17] For these aliphatic polymer blends, the white part was ascribed to PEO and the dark one to PCL. However, it is known that at low magnification (×5000) contrast in TEM is determined by the electron absorbing ability of each component, which is directly related to density, crystallinity, and chemical structure.[28] Considering the higher density and crystallinity of PET (χ = 20% from SI, ρ = 1.38 g cm^{-3})[29] in comparison to PCL (χ = 5% from SI, ρ = 1.145 g cm^{-3}), as well as the fact that aromatic structures would absorb electrons better that aliphatic, it seems logic to ascribe the here-observed darker phase to PET and brighter to PCL [Figure 6(a)]. This observation is much less pronounced when clay is introduced to the polymer blend [Figure 6(b,c)] as expected from the morphology change observed in SEM (Figure 5) and for the clay-containing nanocomposites the filler localization might be difficult to detect [Figure 6(b,b', c,c')]. The C30B stronger affinity toward PET might be ascribed to the presence of two hydroxyl groups in the organomodifier structure and their specific interactions with the carbonyl groups of PET.[27] However, kinetic considerations and operating conditions effects must also be taken into account in the localization.[30] The migration of the nanofiller at the interface can also be related to the thermodynamic effects.[31,32] The localization of C15A layers at the interface of the blend reinforces the interfacial adhesion and thus brings to a better PET/PCL compatibilization. In order to further confirm the TEM observations, theoretical predictions from surface properties might be used.[33]

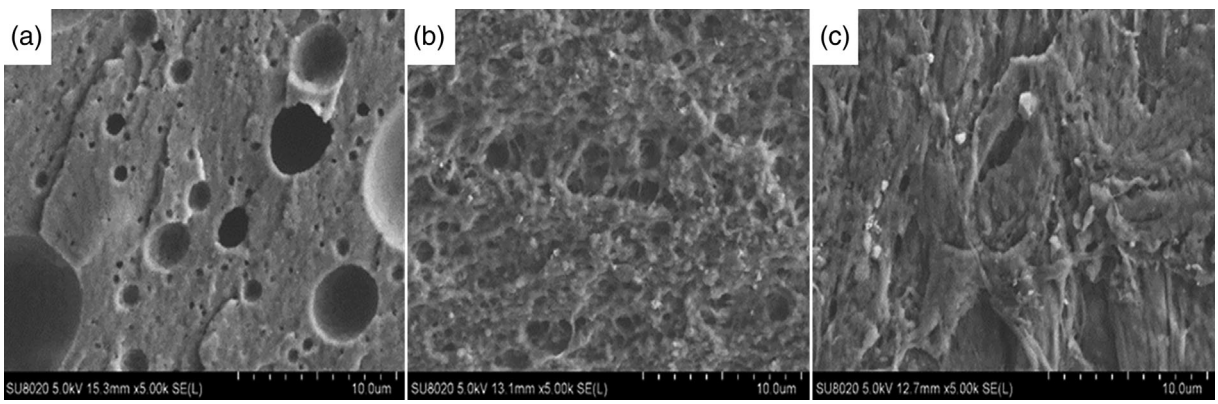

Figure 5. Morphology of fracture surface of (a) 70/30 PET/PCL blends, (b)PET/PCL/C30B and (c) PET/PCL/C15A nanocomposites at 3 wt % Cloisite leading.

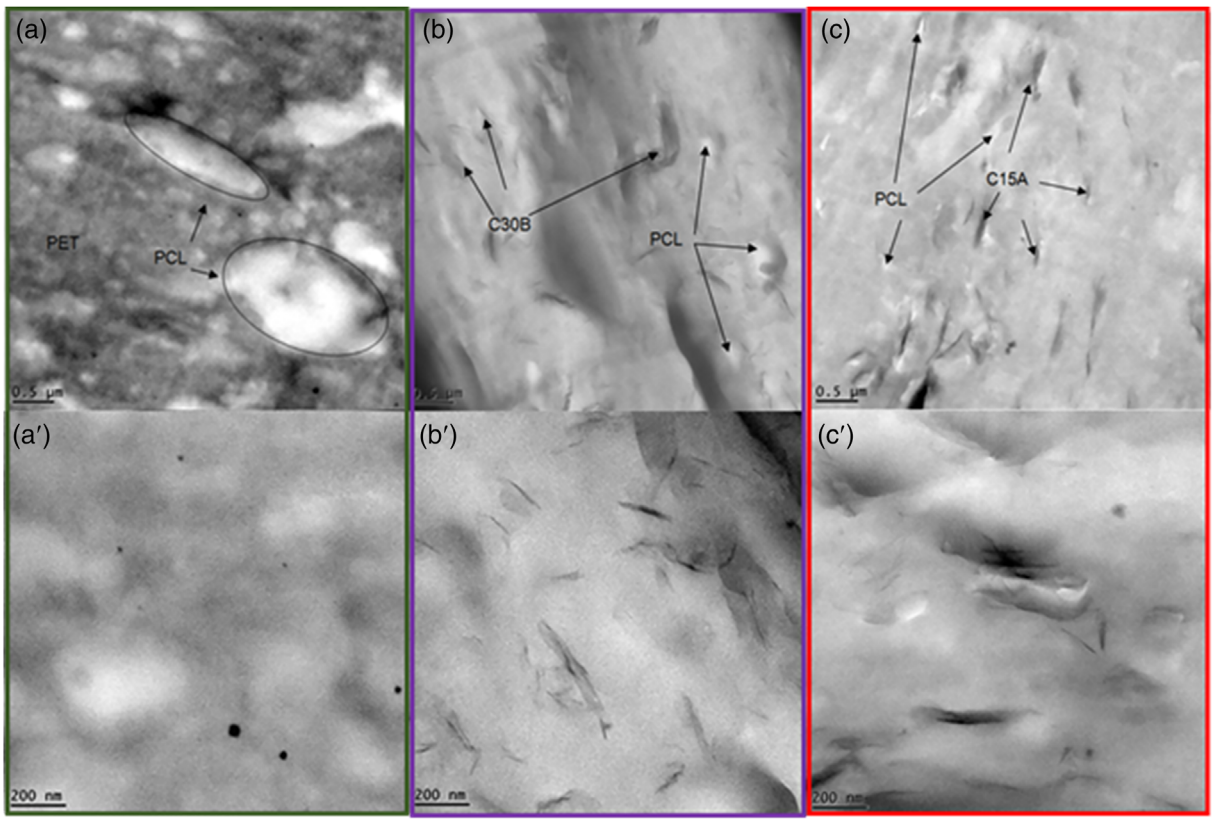

Figure 6. TEM micrographs of (a,a') PET/PCL blend, (b,b') PET/PCL/3C30B nanocomposites, and (c,c') PET/PCL/3C15A nanocomposites (70/30/clays) at different magnifications. [Color figure can be viewed at wileyonlinelibrary.com]

Indeed, nanoclays localization in polymer blends may be predicted through considering the interfacial tensions of the different components. Using Young's equation, it is possible to predict this localization by estimating the wetting parameter ω_a[33] according to eq. 3.

$$\omega_a = \frac{\gamma_{(\text{filler}-\text{PCL})} - \gamma_{(\text{filler}-\text{PET})}}{\gamma_{(\text{PET}-\text{PCL})}} \quad (3)$$

where $\lambda_{(\text{filler-PCL})}$, $\lambda_{(\text{filler-PET})}$, and $\lambda_{(\text{PET-PCL})}$ are the interfacial energies between PCL and filler, PET and filler, PET and PCL, respectively. According to the ω_a value, if $\omega_a > 1$, the clay will be preferentially located in the matrix (PET phase); if $-1 < \omega_a < 1$, the clay will be preferentially located at the interface between the matrix and the dispersed phase and if $\omega_a < -1$, the clay will be preferentially located in the dispersed phase (PCL phase). The surface energies of PET[34] and PCL[35] and the nanoclay C30B,[36] C15A[37] were extrapolated[38] to the melt blending temperature (260 °C) using eqs. (5) and (4) and the values are listed in Table I.

$$-\frac{d\gamma}{dT} = \left(\frac{11}{9}\right) * \left(\frac{\gamma_0}{T_c}\right) * \left(1 - \frac{T}{T_c}\right)^{2/9} \quad (4)$$

$$\gamma = \gamma_0 \times \left(1 - \frac{T}{T_c}\right)^{11/9} \quad (5)$$

where γ_0 is the surface tension at 0 K, T_c is the critical temperature obtained with Lewin *et al*[39] recommendations, and T is the temperature of polymers melt blending (K).

The interfacial tension between polymers and fillers was calculated using the geometric mean approaches[33] eq. (6):

$$\gamma_{12} = \gamma_1 + \gamma_2 - 2 \times \left[\sqrt{\gamma_1^{\text{d}} \times \gamma_2^{\text{d}}} + \sqrt{\gamma_1^{\text{p}} \times \gamma_2^{\text{p}}}\right] \quad (6)$$

where γ_1 and γ_2 are the surface tensions components 1 and 2 respectively; γ_1^d and γ_2^d are the dispersive parts of the surface tensions of components 1 and 2; and γ_1^p and γ_2^p are the polar parts of the surface tension of components 1 and 2.

The wetting parameters were finally determined using eq. (3) and are given in Table II. In the case of PET/PCL/C30B nanocomposite, the wetting parameter is higher than 1 ($\omega_a > 1$)

Table I. Surface Energies of PET, PCL, C30B, and C15A at 260 °C

Materials	γ (mN m^{-1})	γ^{d} (mN m^{-1})	γ^{p} (mN m^{-1})
PET	29.0	22.6	6.5
PCL	31.7	25.5	6.2
C30B	24.3	17.4	6.9
C15A	22.9	21.1	1.7

Table II. Interfacial Tensions and Wetting Coefficients Evaluated at 260 °C

	Geometric mean equation
$\gamma_{PET-PCL(mNm^{-1})}$	0.2
$\gamma_{C30b-PET(mNm^{-1})}$	0.72
$\gamma_{C30b-PCL(mNm^{-1})}$	1.66
ω_a Prediction	4.7 PET phase
$\gamma_{C15A-PET(mNm^{-1})}$	2.71
$\gamma_{C15A-PCL(mNm^{-1})}$	2.89
ω_a Prediction	0.9 Interface

and indicates that C30B could be preferentially located in the PET phase. This result was expected due to the more polar nature of PET relative to PCL. The wetting parameter of PET/PCL/C15A comprised between −1 and +1 indicates that C15A would be localized at the interface between the PET matrix and PCL dispersed phase.

It is worth noting, that TEM also showed the absence of large clay aggregates [Figure 6(b,b', c,c')] and high degree of intercalation/exfoliation is to be expected.

The level of intercalation and exfoliation of the organoclays in PET/PCL blend was investigated using wide-angle X-ray diffraction (WAXD). The WAXD patterns of clay powders and nanocomposite blends with different clay contents are presented in Figure 7. The patterns of both organoclays, C30B and C15A, are identified at 2θ = 4.81° and 2.78°, corresponding to a *d*-spacing of 1.81 nm and 3.17 nm, respectively. Concerning the C30B, the clay incorporation into the PET/PCL blend at 1 wt % increased the d_{001}-spacing from 1.81 to 3.06 nm and did not further vary upon increasing loading [Figure 7(a)]. This observation seems to indicate that high molar mass of polymer chains favor clay delamination in the polymer matrix and results in intercalated like nanocomposites PCL.[40,41] Moreover, the intensity of the 001 diffraction peak increased upon increasing C30B loading, indicating a more extensive domain of periodicity.[41] Intriguingly, the interlayer *d*-spacing of C15A did not significantly change after melt blending with PET/PCL at 1–3 wt % of clay loading [Figure 7(b)]. However, this is not an indication of that intercalation has not occurred. Due to the wide galleries of C15A, the polymer chain could intercalate in the interlayer region.[37] For both nanocomposites, the small peaks at $2\theta = 5.47°$ are related to the 002 plane of the silicate layers dispersed in the matrix.[41]

As the blend morphology and the filler localization influence material properties, the mechanical properties of the PET/PCL/clay nanocomposites were further investigated.

Mechanical properties

The mechanical properties of polymer blends depend on several factors, such as composition and compatibility of the components, incorporation of nanoparticles, blend morphology, and microstructure.[16] Table III and Figure 8 show the tensile properties [Young modulus (MPa), stress at break (MPa), and elongation at break (%)] of the neat PET/PCL blend and of the PET/PCL/clay nanocomposites.

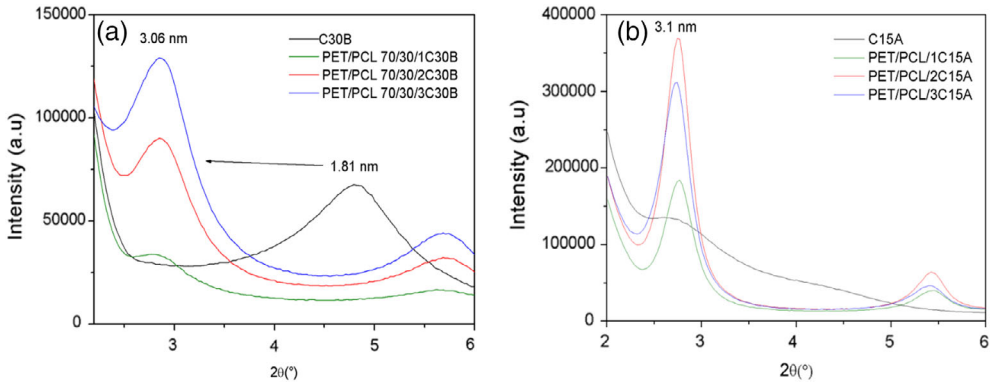

Figure 7. XRD patterns of C30B, PET/PCL/C30B (a) and of C15A, PET/PCL/C15A (b). [Color figure can be viewed at wileyonlinelibrary.com]

Table III. Tensile Mechanical Properties of PET/PCL and PET/PCL/OMMT Blends at Different Clay Concentrations (1–3 wt %)

	Young modulus (MPa)	Yield stress (MPa)	Elongation at break (%)
PET/PCL	1820 ± 4	45.2 ± 0.5	80 ± 10
PET/PCL/1C30B	1866 ± 40	37.7 ± 8	12.9 ± 4
PET/PCL/2C30B	1871 ± 40	40 ± 0.8	15.3 ± 7
PET/PCL/3C30B	1884 ± 36	35 ± 2	17.3 ± 1
PET/PCL/1C15A	1943 ± 74	36 ± 6	15 ± 1
PET/PCL/2C15A	1991 ± 40	36 ± 0.5	12.8 ± 7
PET/PCL/3C15A	2178 ± 50	35.7 ± 1	2.7 ± 0.4

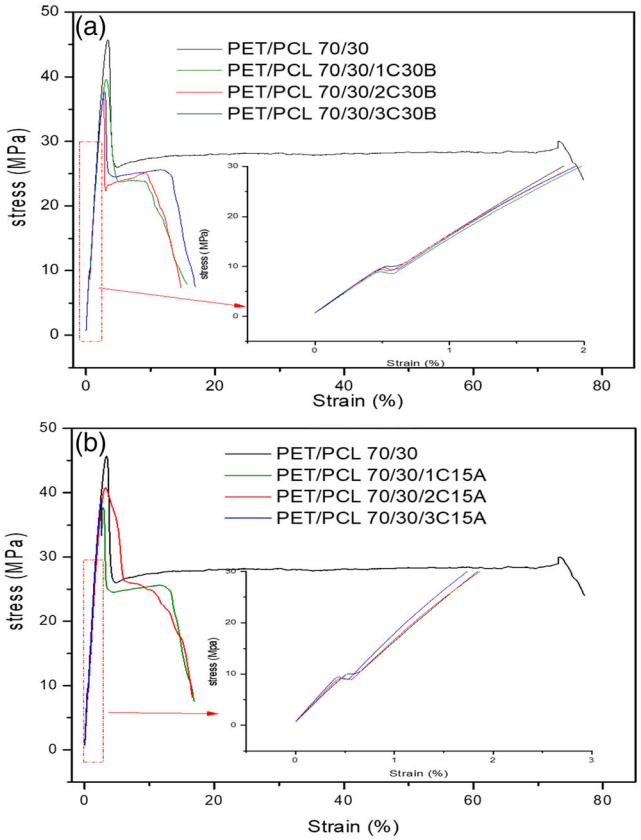

Figure 8. Stress–strain curves of PET/PCL and PET/PCL-based nanocomposites in presence of C30B (a) or C15A (b). [Color figure can be viewed at wileyonlinelibrary.com]

As might be seen, the introduction of C30B into the PET/PCL does not influence the Young's modulus of the material, while somehow reduces the stress at break and more substantially—the elongation at break [Figure 8(a)]. Additionally, the effects seem unaffected by the clay loading. These observations might be explained by the preferential localization of C30B in the PET phase (as shown by TEM and theoretical calculations), clay exfoliation, and three-dimensional network formation, which rigidifies the system. Moreover, the possible presence of hydrogen bondings between the hydroxyl groups of the organomodifier and the carbonyl groups of PET phase might also participate as reported elsewhere.[19,42]

The incorporation of C15A also affects material mechanical properties, although the effects are somehow different from C30B. Indeed, incorporating C15A into the PET/PCL leads to a slight increase in Young's modulus and stress at break, with the expected reduction of elongation at break [Table I and Figure 8 (b)]. These effects become more pronounced as the C15A loading increases and for the PET/PCL/C15A with 3 wt % clay content, the neat PET properties are more or less recovered. The results may be explained by the preferential localization of the nanoclay at the PET/PCL interface, and the thermal stability of these nanoclays (*cf.* SI).

To summarize, according to SEM micrographs, it is clear that the organoclay has an effect of improving the adhesion of the interface, translated by the decrease of PCL domains in the blend nanocomposites. This compatibilizing effect is effectively checked with nanocomposites more rigid than polymer blend (higher Young modulus value). However, the impact of this first level of compatibilization is not enough to balance the negative effect of organoclays on stress and elongation at break and final materials became fragile and lost their flexibility.

Transport properties

The carbon dioxide permeabilities of PCL, PET, PET/PCL blend, and PET/PCL/clays nanocomposites containing 1, 2, and 3 wt %

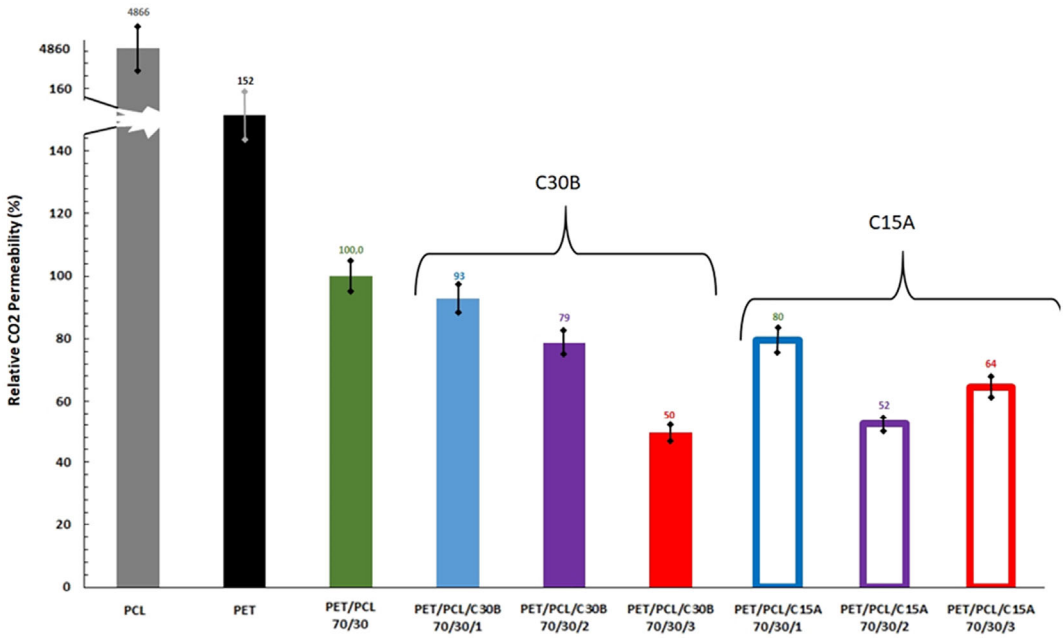

Figure 9. CO_2 gas relatives' permeability of PCL, PET, PET/PCL and PET/PCL-based nanocomposites (PET permeability = 100%). [Color figure can be viewed at wileyonlinelibrary.com]

of inorganic are investigated at room temperature and summarized in Figure 9.

The main aim of PET/PCL blends strategy is to improve the mechanical properties of PET packaging, whereas to preserve or improve CO_2 permeability. So, the relative CO_2 permeabilities with respect to PET has been represented in Figure 9. PCL sample presents a higher CO_2 permeability, that is, more than 60-fold higher than neat PET. The blend PET/PCL (70/30) presents improved CO_2 barrier properties, that is, 44% of permeability compared to PET. The morphological studies [Figure 5(a)] already suggested that two distinct phases with a well-dispersed nodular morphology (as cavities originate from PCL etching) are obtained with PET/PCL (70/30). Based on this, the positive effect on the CO_2 barrier properties might be attributed to the more tortuous path between the most permeable phase (PCL) and the least permeable phase (PET) in the incompatible blend.[43]

In the presence of both C30B and C15A nanoclays, the relative CO2 permeability of PET/PCL blend decreased, thus further improving the gas barrier properties. Generally, with increasing nanoclay content, the barrier properties are expected to be improved, as presented in Figure 9, but the explanation of this barrier properties improved could be due to different causes, that is, crystallinity, nucleating effect.[44–46] More specifically, the relative permeability to PET/PCL (70/30) of the nanocomposites containing 1 and 2 wt % of C30B decreased by 7 and 21%, respectively, while in the blends containing the same compositions of C15A, the permeability showed a decrease of about 20 and 48%, respectively. These results are likely due to the good dispersion/intercalation of these nanoclays at the interface (C15A) and in PET phase (C30B).[47] In the case of the nanocomposite containing 3 wt % C30B, the relative CO2 permeability decreased to 50%, while that of the nanocomposite with 3 wt % C15A decreased to only 35% compared to PET/PCL blend. It is important to stress that this permeation results have also to be, at least partially, attributed to the morphological/interfacial effect of the clays induce the increase of PCL crystallization rate in the nanocomposites[43] (see Supporting information Table S1). So, with the addition of 3 wt % C30B, thus demonstrated best improvement of the barrier properties compared to all other formulations, might be explained with a synergetic effect of (1) the composite microstructures [Figure 5(b)][44–46] (2) the higher PCL crystallization rate (35%) and (3) the co-continuous morphology. Although the permeability to CO_2 in the presence of 3 wt % C15A can likely be assigned to an opposite effect between (1) a higher solubility of CO_2 due to the presence of tactoids or intercalated structures[40,41,44] and (2) a, always, high crystallization rate (32%) but with a different co-continuous morphology [see Supporting information Table S1 and Figure 5(c)].

CONCLUSIONS

In the present work, we successfully prepared a series of PET/PCL (70/30 wt./wt.) nanocomposites including 1–3 wt % of two commercial organoclays (i.e., C30B and C15B) with a panel of tuned properties. The localization of fillers was estimate coming out well into the PET/PCL blend combining TEM analysis and theoretical estimation based on thermodynamic model. The relationship between the type, the content, and the localization of both organoclays on rheological, thermal, mechanical, or CO_2 permeation blends properties were thoughtfully discussed.

The addition of nanoclay into the blend had also a dramatic influence on the rheological properties of the nanocomposites, especially at low-frequency range where the nanocomposites switch the behavior from liquid-like to solid-like behavior for nanoclay content 1–3 wt %, which is indicative of better distribution of the nanoclay in nanocomposites. The C30B was mainly localized in the PET phase and at the PET-PCL interface, whereas the C15A is preferentially present at the interface. SEM analysis allowed to show the influence of different clay localizations on size reduction of dispersed phase domains. From the XRD spectra, it was concluded that an exfoliated and/or intercalated structure for C30B and intercalated structure for C15A in the nanocomposites. From the nanoclays localization and dispersion, the mechanical properties of nanocomposite specimens are enhanced because the clay nanoparticles located at the interface of the mixtures have a compatibilizing effect on interfacial adhesion reinforcement. The results showed significant increase in Young's modulus with 3 wt % of C15A as a result of the good nanoparticle–polymer interaction at the interface. Furthermore, all nanocomposites showed a positive effect to CO_2 barrier properties with a possible tuning on transport properties with type and content of nanofillers. If no nucleation effect has been evidenced in the nanocomposites with nanofillers, an interesting impact of different morphologies on PCL crystallization rate, due to the presence of clays, contributes to mechanical reinforcement and CO_2 permeation improved properties. Therefore, it may be interesting to study the optical properties for opaque packaging applications. Indeed, in the literature, the addition of organomodifed nanoclays to the polymers or polymers blend can affect the optical properties. The first one depends on the dispersion of the nanoclays within the polymer matrix. The optical properties can be deteriorated if there is formation of a larger number of intercalated clay tactoids with greater domain size.[48] Second, the nanoclays give the transparency of the polymer blend when these particles have affinity and exhibit good interaction with the blend components and form a homogeneous morphology.[49] However, it is worth noting that some of mechanical properties enhancement might justify the loss of transparency for some of specific packaging or textile applications.

In the framework of a global investigation of nanocomposites based on PET and/or PET/PCL blends properties including carbon or renewable fillers, this complete study allows to measure and to understand the effect of nanofillers into immiscible but promising blends for large applications as packaging or filtration system.

ACKNOWLEDGMENTS

This work has been supported by between University of Mons (UMONS SMPC) and University of BEJAIA. SMPC laboratory are then gratefully thanked. S. Benali and R. Mincheva acknowledge supports by the European Community (FEDER) for general support in the frame of LCFM-BIOMAT. J.M.R is Chercheur Qualifié from Belgian FNRS agency.

REFERENCES

1. La Mantia, F. P.; Vinci, M. *Polym. Degrad. Stabil.* **1994**, *45*, 121.
2. Srithep, Y.; Javadi, A.; Pilla, S.; Turng, L.; Gong, S.; Clemons, C.; Peng, J. *Polym. Eng. Sci.* **2011**, *51*, 1023.
3. Fuchs, C.; Bhattacharyya, D.; Fakirov, S. *Compos. Sci. Technol.* **2006**, *66*, 3161.
4. Fridrich, K.; Evstatiev, M.; Fakirov, S.; Evstatiev, O.; Ishii, M.; Harrass, M. *Compos. Sci. Technol.* **2005**, *65*, 107.
5. de Mello, D.; Pezzin, S. H.; Amico, S. C. *Polym. Test.* **2009**, *28*, 702.
6. Lim, K. Y.; Chul, K. B.; Yoon, K. *Polym. J.* **2002**, *34*, 313.
7. Ludueña, L. N.; Vázquez, A.; Alvarez, V. A. *J. Appl. Polym. Sci.* **2013**, *128*, 2648.
8. Wu, M.; Shaw, L. L. *J. Power Sources*. **2004**, *136*, 37.
9. Di Lorenzo, M. L.; Paola La Pietra, M. E. E.; Maria Cristina Righetti, M. A. *Polym. Eng. Sci.* **2007**, *47*, 323.
10. Jun, H. S.; Kim, B. O.; Kim, Y. C.; Chang, H. N.; Woo, S. I. *J. Environ. Polym. Degrad.* **1994**, *2*, 9.
11. Lim, K. Y.; Kim, B. C.; Yoon, K. J. *J. Appl. Polym. Sci.* **2003**, *88*, 131.
12. Ma, D.; Zhang, G.; Huang, Z.; Luo, X. *J. Polym. Sci. Part A Polym. Chem.* **1998**, *36*, 2961.
13. Hirotsu, T.; Qi, K.; Nakayama, K. *Polym. Polym. Compos.* **2004**, *12*, 689.
14. Entezam, M.; Khonakdar, H. A.; Yousefi, A. A.; Jafari, S. H.; Wagenknecht, U.; Heinrich, G. *Mater. Des.* **2013**, *45*, 110.
15. Monfared, A.; Jalali-Arani, A. *Appl. Clay Sci.* **2015**, *108*, 1.
16. Ebadi-Dehaghani, H.; Khonakdar, H. A.; Barikani, M.; Jafari, S. H. *Compos. Part B Eng.* **2014**, *69*, 133.
17. Fang, Z.; Harrats, C.; Moussaif, N.; Groeninckx, G. *J. Appl. Polym. Sci.* **2007**, *106*, 3125.
18. As'habi, L.; Jafari, S. H.; Khonakdar, H. A.; Boldt, R.; Wagenknecht, U.; Heinrich, G. *Express Polym. Lett.* **2013**, *7*, 21.
19. Yousfi, M.; Soulestin, J.; Lacrampe, M. F.; Vergnes, B. In PPS-27, 2011, 27th World Congress of the Polymer Processing Society, May 10–14, Marrakech, Morocco; **2014**, p 1.
20. Chiellini, E.; Corti, A.; Giovannini, A.; Narducci, P.; Paparella, A. M.; Solaro, R. *J. Environ. Polym. Degrad.* **1996**, *4*, 37.
21. Rinawa, K.; Maiti, S. N.; Sonnier, R.; Lopez Cuesta, J. M. *Polym. Bull.* **2015**, *72*, 3305.
22. Issaadi, K.; Habi, A.; Grohens, Y.; Pillin, I. *Appl. Clay Sci.* **2015**, *107*, 1.
23. Seddik, B.; Pillin, I.; Habi, A.; Grohens, Y. *Appl. Clay Sci.* **2015**, *116–117*, 69.
24. Joshi, M.; Butola, B. S.; Simon, G.; Kukaleva, N. *Macromolecules*. **2006**, *39*, 1839.
25. Sinha Ray, S.; Pouliot, S.; Bousmina, M.; Utracki, L. A. *Polymer*. **2004**, *45*, 8403.
26. Ray, S. S.; Bousmina, M. *Polymer*. **2005**, *46*, 12430.
27. Kim, S.; Lofgren, E. A.; Jabarin, S. A. *J. Appl. Polym. Sci.* **2013**, *127*, 2201.
28. Fultz, B.; Howe, J. Transmission Electron Microscopy and Diffractometry of Materials, 3rd ed.; Springer-Verlag: Berlin Heidelberg, **2008**.
29. Larranaya, M. D.; Lewis, R. J.; Lewis, R. A. Hawley's Condensed Chemical Dictionary, 16th ed.; John Wiley & Sons: New Jersey, USA, **2016**; p 1568.
30. Taguet, A.; Cassagnau, P.; Lopez-Cuesta, J.-M. *Prog. Polym. Sci.* **2014**, *39*, 1526.
31. Balazs, A. C.; Emrick, T.; Russell, T. P. *Science*. **2006**, *314*, 1107.
32. Araki, T.; Tanaka, H. *Phys. Rev. E*. **2006**, *73*, 061506.
33. Cardinaud, R.; Mcnally, T. *Eur. Polym. J.* **2013**, *49*, 1287.
34. Li, W.; Karger-Kocsis, J.; Schlarb, A. K. *Macromol. Mater. Eng.* **2009**, *294*, 582.
35. Li, L.; Ruan, W.-H.; Zhang, M.-Q.; Rong, M.-Z. *Express Polym. Lett.* **2015**, *9*, 77.
36. Entezam, M.; Khonakdar, H. A.; Yousefi, A. A.; Jafari, S. H.; Wagenknecht, U.; Heinrich, G. *Macromol. Mater. Eng.* **2013**, *298*, 113.
37. Yousfi, M.; Soulestin, J.; Vergnes, B.; Lacrampe, M. F.; Krawczak, P. *Macromol. Mater. Eng.* **2013**, *298*, 757.
38. Wu, S. Polymer Interface and Adhesion. 1st ed.; Routledge: New York, **2017**.
39. Lewin, M.; Mey-Marom, A.; Frank, R. *Polym. Adv. Technol.* **2005**, *16*, 429.
40. Broekaert, C.; Peeterbroeck, S.; Benali, S.; Monteverde, F.; Bonnaud, L.; Alexandre, M.; Dubois, P. *Eur. Polym. J.* **2007**, *43*, 4160.
41. Ghanbari, A.; Heuzey, M. C.; Carreau, P. J.; Ton-That, M. T. *Rheol. Acta*. **2013**, *52*, 59.
42. Yousfi, M.; Lepretre, S.; Soulestin, J.; Vergnes, B.; Lacrampe, M. F.; Krawczak, P. *J. Appl. Polym. Sci.* **2014**, *131*, 1.
43. Motta, O.; Di Maio, L.; Incarnato, L.; Acierno, D. *Polymer*. **1996**, *37*, 2373.
44. Gain, O.; Espuche, E.; Pollet, E.; Alexandre, M.; Dubois, P. *J. Polym. Sci. Part B Polym. Phys.* **2005**, *43*, 205.
45. Bitinis, N.; Verdejo, R.; Maya, E. M.; Espuche, E.; Cassagnau, P.; Lopez-Manchado, M. A. *Compos. Sci. Technol.* **2012**, *72*, 305.
46. Adewole, J. K.; Jensen, L.; Al-Mubaiyedh, U. A.; Von Solms, N.; Hussein, I. A. *J. Polym. Res.* **2012**, *19*, 9814.
47. Stamm, M. In Polymer Surfaces and Interfaces; Stamm, M., Ed.; Springer: Berlin, Heidelberg, **2008**.
48. Kim, S. W.; Cha, S. H. *J. Appl. Polym. Sci.* **2014**, *131*, 1.
49. Singh, A. K.; Prakash, R.; Pandey, D. *RSC Adv.* **2013**, *3*, 15411.